*Journal of The Electrochemical Society*, **147** (11) 4374-4378 (2000)
S0013-4651(00)01-118-6 CCC: $7.00 

# Characteristics of Multilayered Barium Titanate Films and Their Effect on Thin-Film Electroluminescent Cells

**Yun-Hi Lee,[a,z] Jung-Hoon Oh,[b] Byeong-Kwon Ju,[a] and Myung-Hwan Oh[a]**

[a]*Korea Institute of Science and Technology, Seoul, Korea*
[b]*Samsung Electronics, Suwon, Korea*

In this work, we fabricated thin-film electroluminescent (TFEL) cells with a new multilayered $BaTiO_3$ layer for the low-voltage-driven devices. At first, we performed the voltage accelerated breakdown testing of the multilayered $BaTiO_3$ having both high dielectric constant and high breakdown strength. The time-zero-breakdown distribution is shown to be dependent on surface roughness, while the long-term failure studied by time-dependent dielectric breakdown technique at high field is dependent on the bulk characteristics, *i.e.,* transition layer within multilayered $BaTiO_3$ (m-BT) films. Second, the TFEL devices were prepared using the multilayered $BaTiO_3$ as dielectric materials. We observed a decrease of turn-on voltage with increasing thickness and increase of the maximum overvoltage. Third, typical symmetric capacitance-voltage and internal charge-phosphor field characteristics were obtained for the device with thin m-BT layers. With increasing thickness of m-BT the significant asymmetry with respect to the applied voltage polarity was observed. This is a main difference as compared with the symmetric characteristics of conventional TFEL devices with low dielectric constant insulators. The experimental results indicate that a selection of the thickness of upper m-BT and their deposition process would strongly affect the interfacial characteristics as well as bulk characteristics of an as-grown ZnS:Pr,Ce layer.


Manuscript submitted January 27, 2000; revised manuscript received July 31, 2000.

The insulators in alternating current thin-film electroluminescent (ACTFEL) cells should have high dielectric reliability as well as a high figure of merit in order to achieve both low power consumption and stable operation of the device. A large insulator capacitance increases the voltage drop across the phosphor layer, thus increasing the magnitude of the phosphor field.[1] A large phosphor field effectively contributes to the emission of deep interface traps into the phosphor conduction band and a large phosphor field enhances the acceleration process of the injected electrons as they are transported across the phosphor. Also, a large insulator capacitance also reduces the operating voltage.

The larger the breakdown field in insulating layers, the higher the applied voltage the device can withstand and the more reliable the device. Unfortunately, the high dielectric constant materials tend to have low breakdown field strength. Thus, we can imagine that one of the methods of increasing the dielectric constant while maintaining a large breakdown field is to use alternating layers of one material with a large breakdown field and another material with a high dielectric constant.[2,3] When a polycrystalline $BaTiO_3$ film (p-BT), having a high dielectric constant but relatively low breakdown field, was used as an insulating layer for electroluminescent devices (ELDs), it was found that the efficiency of the device decreases because of the high leakage current of the p-BT layer. However, a recent work has shown that, by a new stacking method, multilayered $BaTiO_3$ (m-BT) films can be fabricated where both the high dielectric constant ($\sim$100 at 1 kHz) and high dielectric breakdown strength are achievable features.[4] Furthermore, this study has presented that an m-BT film can be successfully applied to the lower insulating layer for highly efficient thin-film electroluminescent devices (TFELD).

In this work, we summarize the results of dielectric reliability of the m-BT films evaluated using two techniques, time-zero-dielectric-breakdown (TZDB) and time-dependent-dielectric breakdown (TDDB).[5] As one of conclusions, we suggest that the "transition layer" within m-BT is a figure of merit in determining whether an m-BT layer provides sufficient margins to guarantee dielectric reliability. Results from capacitance-voltage (C-V) and internal charge ($Q_{int}$) phosphor field ($F_p$) analysis are used to investigate the effect of different thicknesses of m-BTs on the electrical behavior and the maximum overvoltage margins of TFEL cells. The surface roughness estimated by atomic force microscopy (AFM) was used to understand the C-V abruptness. Finally, we present an Auger electron spectroscopy (AES) spectrum of TFEL cells with different m-BT films, accounting for the effect of m-BT thickness on both interfaces between m-BT and ZnS:Pr,Ce. This result enables the explanation of the strong asymmetric properties for the upper interface and helps to determine the usable thickness for manufacturing reliable TFEL devices using high dielectric constant insulators.

[z] E-mail: lyh@kist.re.kr

## Fabrication and Characterization

In order to measure dielectric reliability of our multilayered-$BaTiO_3$, ramp-voltage-stresses *I-V* (TZDB) and constant-voltage-stresses *I-t* (TDDB) characteristics were taken by a fully automated Keithley 237 high-voltage source and measure unit. In this measurement the breakdown field of an M (ITO) - I (m-BT) – M (Al) capacitor was defined as the applied field at which the leakage current exceeded 1 mA. Time-to-breakdown was monitored over the time interval of 0-1000 s for the 180 dot capacitors with a dot area of $3.8 \times 10^{-3}$ cm$^2$. An impedance analyzer (HP 4192A) was used to obtain ac dielectric properties such as dielectric constant and dielectric loss as a function of the applied frequency for the m-BT.

Electroluminescent (EL) cells are fabricated by electron-beam evaporation in the stack configuration in which a ZnS:Pr, Ce layer is sandwiched between layers of m-BT and m-BT which are contacted by a bottom indium thin oxide (ITO) and a top aluminum (Al) electrode. The ZnS:Pr, Ce phosphor thickness was approximately constant for all of these EL devices. The m-BT as upper and lower insulator were varied about 200, 400, and 700 nm. The symmetric ac TFEL cells of ITO/m-BT (200, 400, 700 nm)/ZnS:Pr,Ce (450 nm)/ m-BT (200, 400, 700 nm)/ Al are referred to as "s1," "s2," and "s3," respectively, in the remainder of this paper.

C-V and $Q$-$F_p$ analysis is accomplished using a programmable arbitrary waveform generator (HP model 33120A) and a high-voltage amplifier (Apex model PA 85). All the electrical data were obtained using a digitizing oscilloscope (Tektronix model 510A). The C-V and internal charge ($Q_p$) phosphor field ($F_p$) characteristics were monitored by plotting the dynamic capacitance as a function of the voltage across the EL devices and analysis is made by the $Q_p(t)$ and $F_p(t)$ equations.[6,7]

## Results and Discussion

*Characteristics of m-BT films under the accelerated dc stress.*—Figure 1 shows a close look at breakdown with scanning electron microscope (SEM) measurements for three different types of m-BT. SEM pictures of the breakdown site clearly show the m-

S0013-4651(00)01-118-6 CCC: $7.00 

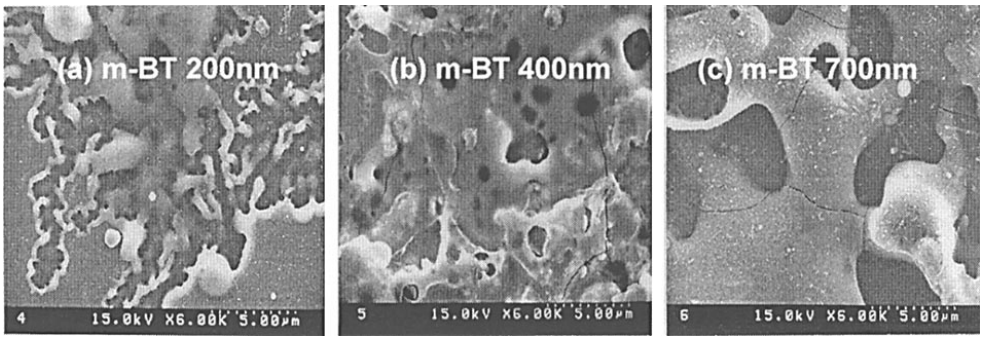


**Figure 1.** SEM photographs for the breakdown site for the m-BT with different thicknesses.

BT destroyed by thermal runaway effects. The m-BT with a thicker p-BT underlayer has deeper hole and severe crackings.

As generally known, the breakdown is studied under the accelerating test condition of high field stress resulting in practically measurable breakdown time.[8] In order to extrapolate the dc acceleration results to field conditions as are found in common ac EL device application, a knowledge of TDDB behavior is necessary. A probability distribution function that fits breakdown data can be used to predict failure rates as a function of time. Gaussian (or normal) distribution is a bell-shaped curve used for process monitoring and control charts. Weibull distribution is similar to log normal distribution and is appropriate for accelerated life testing as well as predicting early failure.

Figures 2 and 3 show time-zero current (*I*) electric field (*E*) characteristics and the time-zero-breakdown distribution for three types of m-BT at constant time, respectively. The leakage current at the fixed stress field decreased as thickness of m-BT increased and the most frequent breakdown of 700 nm thick m-BT occurred at the lower electric field when compared with those of the thinner m-BTs. Furthermore, Fig. 3 of TZDB results in ramp-voltage stress for the 400 and 700 thick m-BT films, showing typical Weibull distribution applicable to failure in good insulating films.[9] Figure 4 shows a typical cumulative Weibull plot for three types of m-BT. Here, the horizontal axis represents the stress time *t* and the vertical axis represents the cumulative failure percent. Note that the lifetime increases slightly as the thickness of m-BT is increased.

It is generally accepted that an extrinsic breakdown is the largest reliability problem for the oxide insulating film and the extrinsic breakdown is related to defects which exist in the film before the electric stress, *i.e.*, process-induced defects such as particle, surface asperities, and structural weakness.[8,10] Here, in order to study the factor influencing the results presented in Fig. 1-4, we investigate especially the interface roughness effect on the peak occurrence of time zero breakdown and the layered structural effect of m-BT, *i.e.*, thickness of the transition layer between p-BT and a-BT, on the leakage current and TDDB properties with increasing thickness. Figure 5 shows AFM images for the surface of m-BT films. Root-mean-square (rms) roughness estimated from these results increases with increasing thickness of m-BT, indicating that the roughness of m-BT is increased by forming a thicker p-BT underlayer. Thus, based on the explanation that the nonuniformity and the sharp points are assumed to be main sources of the weak spot under the dc electric field of 1-2 MV/cm, the trends of Fig. 3 and 4a can be easily understood.

*Role of the transition layer within m-BT on the long-life-breakdown behavior of m-BT capacitors.*—The reduced leakage current with increasing thickness as shown in Fig. 1 could not be explained considering the increase of rms roughness. Here, it should be emphasized that the increase of p-BT thickness is always accompanied by an increase of the transition layer between p-BT and an a-BT layer, as shown in Ref. 5. The decrease of leakage current at dc high stress voltage is most likely due to the thicker transition layer with increasing p-BT thickness, supporting the previous suggestion that the transition layer resists electron movement.[4]

In the same context, the shift of the Weibull plot toward longer time with increasing thickness in Fig 4b can be attributed to both the

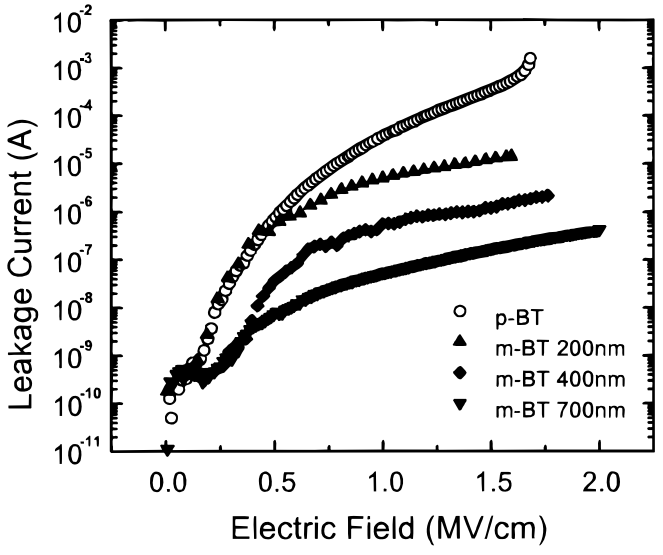


**Figure 2.** DC leakage current-applied field curves for the m-BT with different thicknesses after short-term aging.

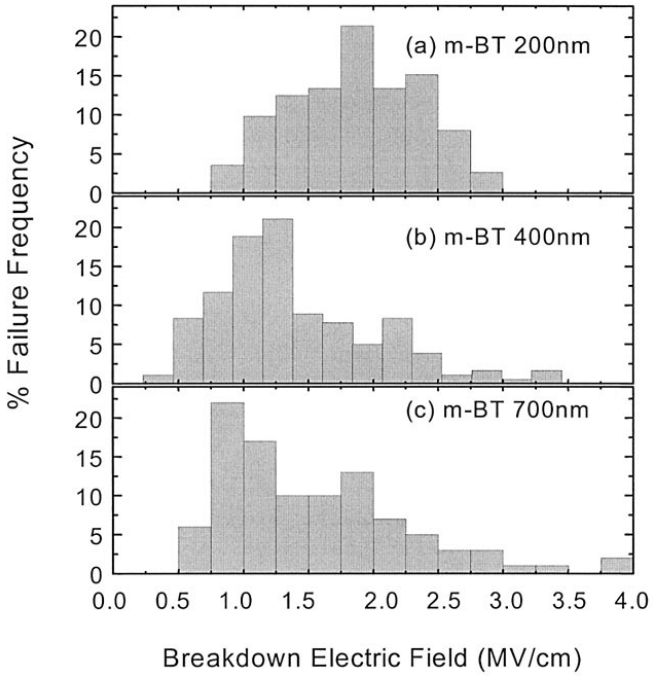


**Figure 3.** Breakdown field histogram for the m-BT with different thicknesses.

S0013-4651(00)01-118-6 CCC: $7.00 

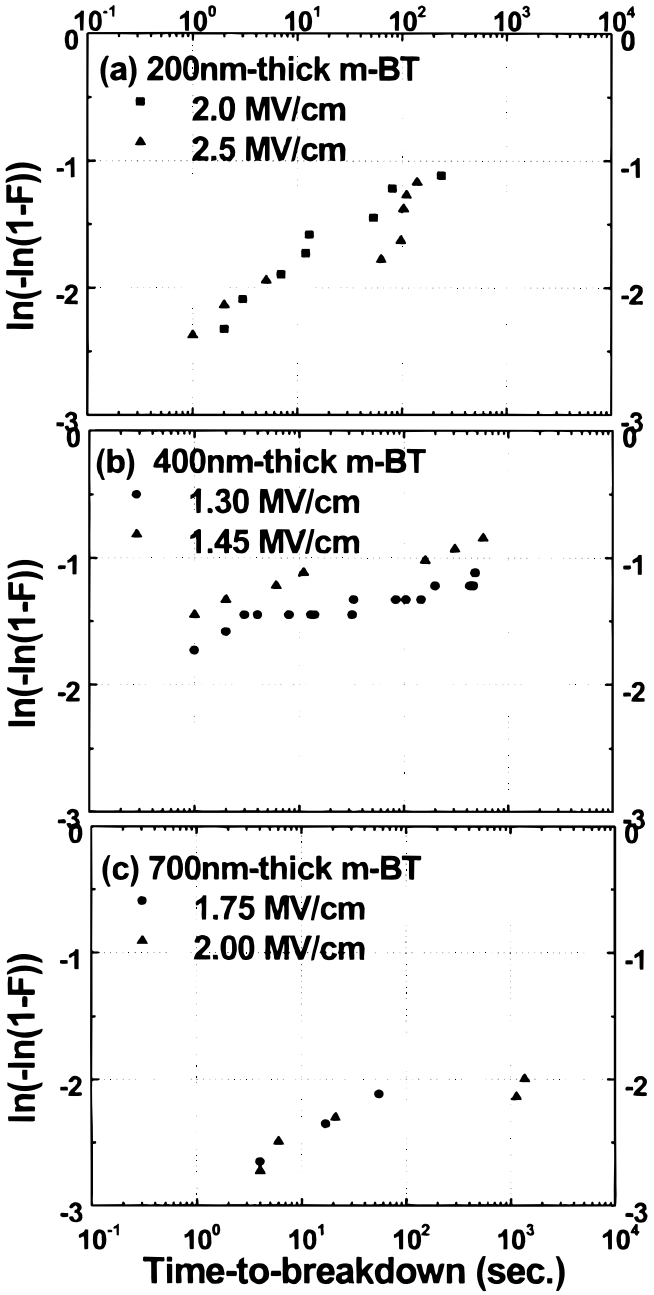


**Figure 4.** TDDB time-to-failure distribution for m-BT with different thickness under negative bias. Usually the cumulative distribution function [$F(t)$] is plotted and the breakdown data are often approximately Weibull distributed. $F(t) = 1 - \exp(-t/\eta)\,\beta$ where $t$, $\beta$, and $\eta$ represent time, shape parameter, and characteristic time to failure.

stress relaxation and a reduction of moving oxygen vacancies by the widening of the transition region between p-BT and a-BT.

*C-V and $Q_{int}$-$F_p$ characteristics of TFEL cells under bipolar pulse drive.*—Note that the C-V curve of our EL devices shifts in a slightly nonrigid manner with respect to m-BT thickness as shown in Fig. 6a. This nonrigid shift in the C-V curve indicates that the interface state density in the preclamping field regime,[6] $Q_{ss}$, is dependent on the m-BT thickness. The variation of rms roughness with increasing thickness of m-BT is seen as the source of the change of $Q_{ss}$. Note from the the figure that $C_i$ (Al plus) is greater than $C_i$ (Al minus). A family of C-V curves for the devices with 400 and 700 nm thick m-BT are displayed as a function of operating voltage in Fig. 6b and c, respectively. Perhaps the most unusual aspects of the curves shown in these figures are the significant asymmetry with respect to the applied voltage polarity for all symmetric devices fabricated in this work. Furthermore, the most significant asymmetry was observed at an "s3" device. Tentatively, we attribute the observed polarity-dependence of $C_i$ to the existence of different interface state distributions at the two interfaces between the phosphor and insulators, and thus, interface roughness.

Next, we present the typical results of $Q$-$F_p$ measurements for the s1, s2, and s3 devices in Fig. 7. There are several differences between these devices. At first, much more conduction charge is transported across the phosphor in the s3 device. This is a consequence of the larger dielectric capacitance of m-BT of the s3 device (*i.e.*, ~95) compared to those of s1 (~20) and s2 (55 ~ 65). Second, contribution of relaxation charge to conduction charge is larger in s2 and s3. Much of the charge across the phosphor of s2, and s3 appears to reside in deep traps such that it is emitted from these traps when the external bias is maintained at peak voltage. Third, the s1, s2, and s3 device exhibit a distinct steady-state field of $F_{ss}^{+}$ (Al plus). In contrast, $F_{ss}^{-}$ of s2 and s3 at Al minus is not well-defined as well as the magnitude and shape, as shown in Fig. 8. Finally, the $Q$-$F_p$ plot at Al minus is nearly symmetric for the s1 device but strongly asymmetric for the s2 and s3.

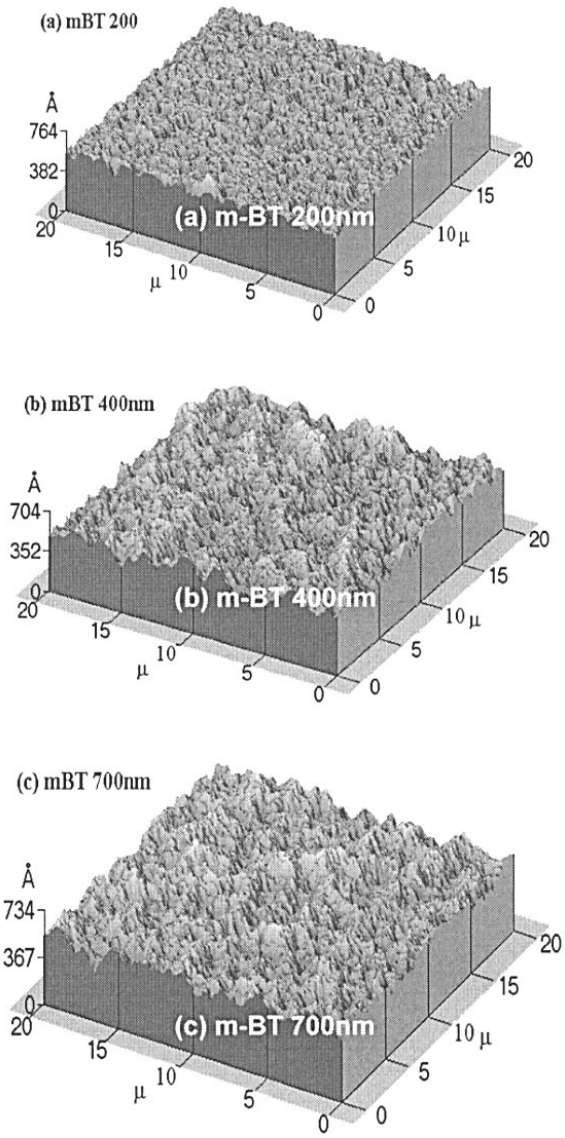


**Figure 5.** AFM images for the topmost surface of m-BT with different thicknesses.

S0013-4651(00)01-118-6 CCC: $7.00 

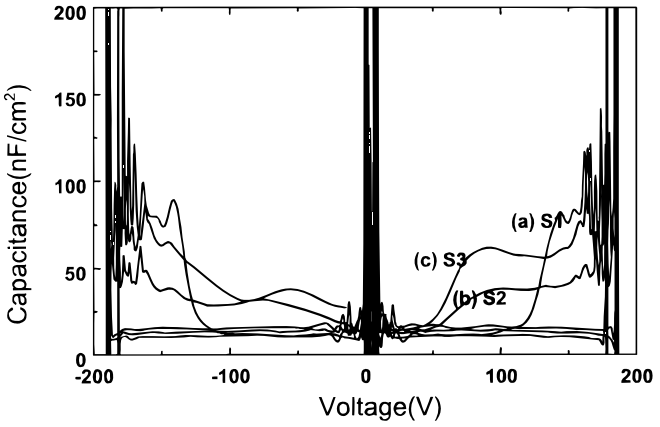


**Figure 6.** Capacitance-voltage curves of EL devices with different thickness of m-BT.

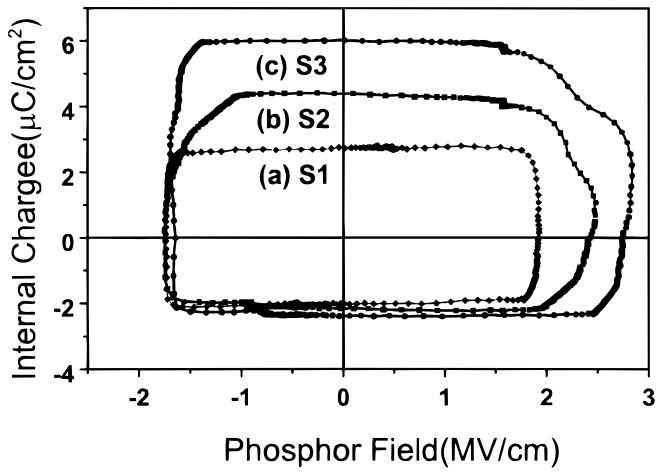


**Figure 7.** Internal charge ($Q_{int}$)-phosphor field ($F_p$) loops of the s1, s2, and s3 devices.

From the observed results, we suppose that while the bottom interface is relatively independent of the lower m-BT layer, the top interface is severely affected by the thickness of m-BT or their processing. Other evidence is shown in Fig. 8. $F_{ss}^{+}$ ( ITO minus) for the s2 is nearly constant except at larger $V_{max}$ ($V_{max}$ = 220 V), while $F_{ss}^{-}$ (*i.e.*, electron emitted from Al side interface) increases continuously with increasing $V_{max}$. The strong asymmetry trends exhibited by the internal phosphor field ($F_p$) are attributed to an interface state distribution of the bottom interface which sharply increases at a certain energy to a large density as compared to those of the top interface. This contention, that the interface state distribution is abrupt for the bottom interface, is supported by the $Q_{ss}$ trends shown in Fig. 5 and 6 and sharper interfacial profiles confirmed by AES analysis.

In contrast, the $F_{ss}^{-}$ trends shown in Fig. 8 and 9 indicate that field-clamping does not occur when electrons are emitted from the top interface. It is possible that this absence of field-clamping arises from shallow interface states that are distributed over a large range of energy.

Finally, to confirm the internal asymmetric properties of the devices with the symmetric material and thickness, we measured the in-depth profile using AES. Figure 9a-c shows an entire concentration profile of the composing ions for the s1, s2, and s3 devices, respectively, revealing three features. First, the amount of Zn and Ba

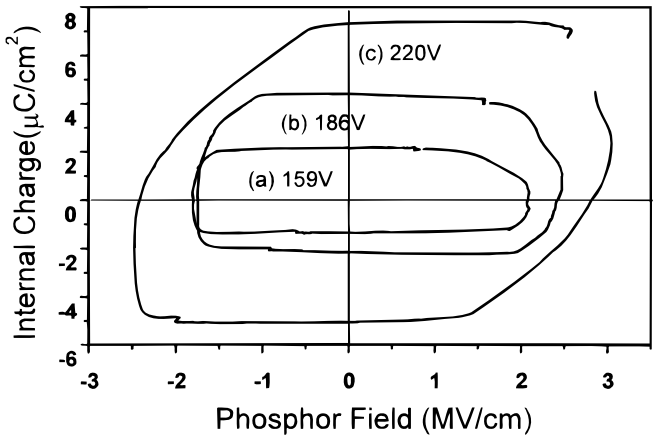


**Figure 8.** Internal charge ($Q_{int}$)-phosphor field ($F_p$) loops as a function of maximum applied voltage.

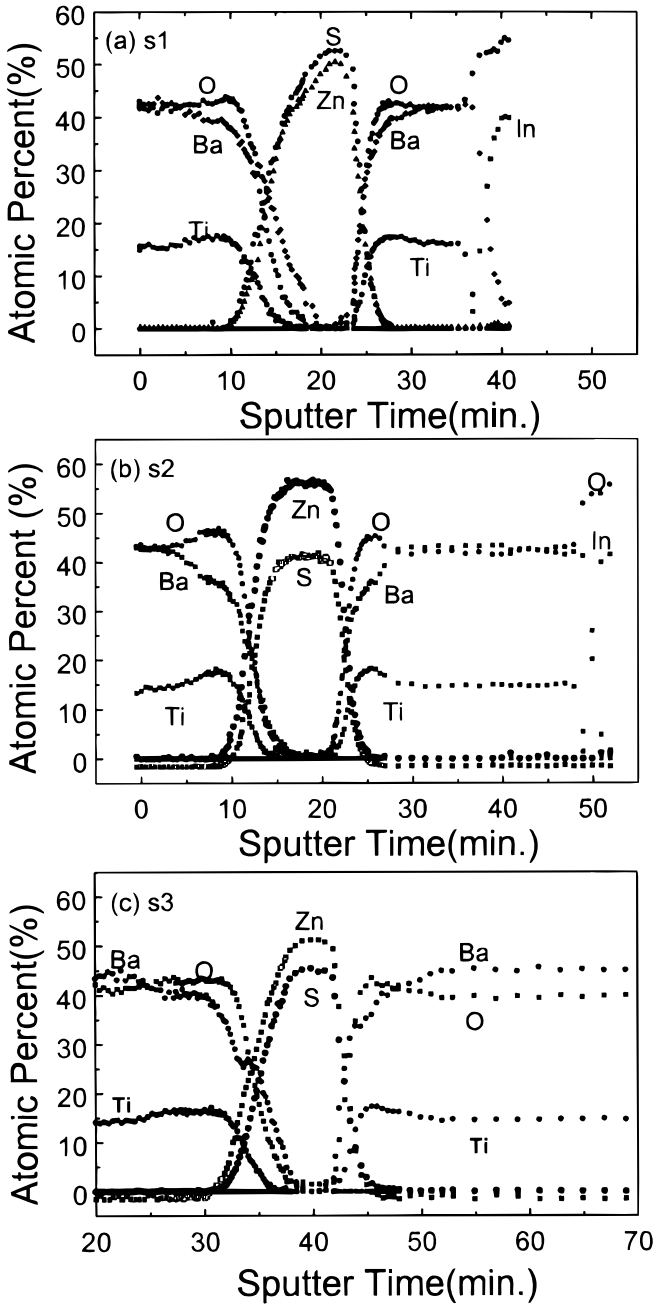


**Figure 9.** AES depth profile for the EL structure with different thicknesses of m-BT.

S0013-4651(00)01-118-6 CCC: $7.00 

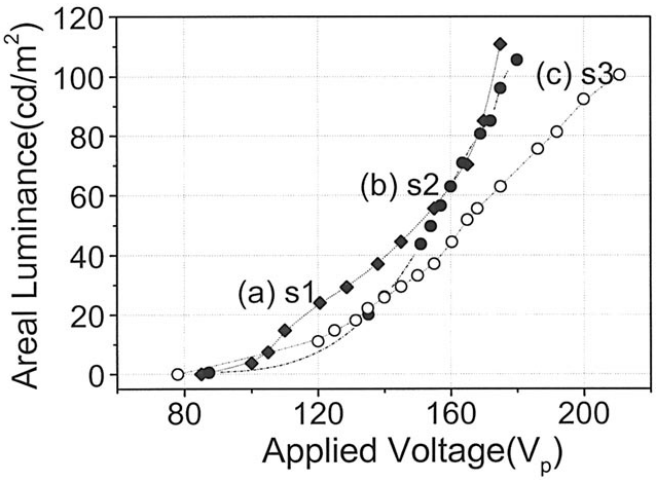


**Figure 10.** Luminance-applied voltage curves of the s1, s2, and s3 devices, respectively. Prior to starting measurement, EL devices were aged for about 90 min to stabilize. The waveform applied is nearly symmetric bipolar pulses of rectangular shape with a pulse with of 50 μs and a frequency of 1 kHz.

was slightly higher than S and O at the lower interface between lower m-BT and ZnS:Pr,Ce, regardless of the thickness of m-BTs. Second, differing from the lower interface, the ratio of Zn to S at the upper interface was significantly varied from sulfur-rich s1 to sulfur deficient s2 and s3. As frequently observed, the off-stoichiometric ZnS, *i.e.*, Zn excess (or sulfur deficient) easily resulted from the phosphor process, although controllability was dependent on the physical vapor deposition or chemical vapor deposition. Here, it is important that the ratio of S/Zn of the s1 device was higher than 1 after deposition of the upper insulator followed by vacuum-anneal of ZnS, while that of s2 and s3 was lower than unity. Also, note that at the top interface region the layered interface was formed such as Ba-rich m-BT, a Zn-rich region, and their mixed region. It was common to the s2 and s3 devices.

*Luminance applied voltage characteristics of TFEL cells using the m-BT insulator.*—The luminance-applied voltage curves of the s1, s2, and s3 devices are shown in Fig. 10. This figure shows two distinct features. First, there is a decrease of threshold voltage with increasing m-BT thickness, *i.e.*, dielectric capacitance. Essentially, the reason for this result is that with increasing insulator dielectric capacitance there is an increasing portion of the applied voltage which appears across the phosphor layer, when the same value of $V_a$ was applied at the devices. Second, there is an increase of maximum overvoltage margin with increasing m-BT thickness. It is proposed that the thicker insulating layer has a beneficial influence on the operation reliability of TFEL devices.

An asymmetric TFEL device with different thick lower and upper m-BT is necessary for a complete evaluation of TFEL devices using these dielectrics.

## Conclusions

In this work, we applied successfully a high dielectric constant material for the insulator of low voltage-driven white-light emitting ac TFEL devices. The TZDB and TDDB techniques were employed as methods of investigating dielectric reliability for TFELDs. The value of the most frequent breakdown field was lowered with increasing thickness of m-BT, while distribution of the breakdown field was narrowed for thinner film. Analysis of the surface roughness for the m-BT confirmed that the time-zero breakdown mechanism is related to the rms deviation of roughness. The reduced dc leakage current at the thick m-BT and the long-time to failure were related to the presence of a wide transition layer formed between poly- and amorphous-BT. Therefore, we suggest that the width of "transition layer" in m-BT be a figure of merit in determining whether an m-BT layer provides sufficient margins to guarantee dielectric reliability.

For our symmetric TFEL devices using the high dielectric layers, the most distinct feature of the C-V and $Q$-$F_p$ characteristics is the significant asymmetry with respect to the applied voltage polarity. The top interface is severely affected by the type of m-BT, whereas the bottom interface is relatively independent of the lower dielectric layer. The luminance-voltage characteristics show two distinct features; a decrease of threshold voltage with increasing m-BT thickness, *i.e.*, dielectric capacitance, and the increase of maximum over voltage margin with increasing m-BT thickness. It is proposed that the thicker insulating layers have a beneficial influence on the operation reliability of TFEL devices.

*The Korea Institute of Science and Technology assisted in meeting the publication costs of this article.*

## References

1. Y. H. Lee, Y. S. Kim, B. K. Ju, and M. H. Oh, *IEEE Trans. Electron Devices*, **ED-46,** 892 (1999).
2. M. H. Song, Y. H. Lee, T. S. Hahn, and M. H. Oh, *J. Cryst. Growth*, **167,** 157 (1996).
3. M. H. Song, Y. H. Lee, T. S. Hahn, K. H. Yoon, and M. H. Oh, *J. Kor. Ceram. Soc.*, **32,** 761 (1995).
4. M. H. Song, Y. H. Lee, T. S. Hahn, and M. H. Oh, *J. Appl. Phys.*, **79,** 3744 (1996).
5. J. H. Oh, Y. H. Lee, B. K. Ju, C. Y. Park, and M. H. Oh, *J. Appl. Phys.*, **82,** 6203 (1997).
6. A. Abu-Dayah, S. Kobashi, and J. F. Wager, *Appl. Phys. Lett.*, **62,** 744 (1993).
7. R. C. McArthur, J. D. Davison, and J. F. Wager, *Appl. Phys. Lett.*, **56,** 1889 (1990).
8. J. C. Lee, I. C. Chen, and H. Hu, *IEEE Trans. Electron Devices*, **ED-35,** 2268 (1988).
9. A. B. Joshi, D. L. Kwong, and S. Lee, *Appl. Phys. Lett.*, **60,** 1489 (1992).
10. K. F. Schuegrat and C. Hu, *International Reliability Physics Proceedings*, p. 120 (1994).